British Journal of Mathematics & Computer Science
14(6): 1-17, 2016, Article no.BJMCS.23221
ISSN: 2231-0851

SCIENCEDOMAIN *international*
www.sciencedomain.org

Oscillatory Blood Flow in Convergent and Divergent Channels, Part 1: Effects of Pulse Amplitude and Local Constriction Height

W. I. A. Okuyade[1*] and T. M. Abbey[2]

[1]Department of Mathematics and Statistics, University of Port Harcourt, Port Harcourt, Nigeria.
[2]Department of Physics, Applied Mathematics and Theoretical Physics Group, University of Port Harcourt, Port Harcourt, Nigeria.

Authors' contributions

This work was carried out in collaboration between authors WIAO and TMA. Author TMA designed the study, wrote the protocol and supervised the work. Author WIAO wrote the introduction and solved the problem under the guidance of author TMA. Author TMA did the programming for the results while author WIAO managed the analyses of the study under author TMA supervision. Author WIAO wrote the first draft of the manuscript, managed the literature searches and edited the manuscript. Both authors read and approved the final manuscript.

Article Information

DOI: 10.9734/BJMCS/2016/23221
Editor(s):
(1) Raducanu Razvan, Department of Applied Mathematics, Al. I. Cuza University, Romania.
Reviewers:
(1) Anonymous, University of Hacettepe, Ankara, Turkey.
(2) Mohammed Abdulhameed, Federal Polytechnic, Bauchi, Nigeria.
(3) Grienggrai Rajchakit, Maejo University, Thailand.
(4) Alal Hosen, Rajshahi University of Engineering and Technology, Bangladesh.
Complete Peer review History: http://sciencedomain.org/review-history/13474

Original Research Article

Received: 21st November 2015
Accepted: 4th January 2016
Published: 27th February 2016

Abstract

Oscillatory blood flow in convergent and divergent channels is investigated. The problem which involves a set of non-linear differential equations is handled analytically using the method of regular perturbation series solutions. Solutions are obtained for the velocities, pressure and wall shear stress, and are analyzed graphically. It is found that the variations in the pulse amplitude and height of constriction reduce the axial velocity and pressure but increase the radial velocity and wall shear stress. More so, it is observed that flow separation occurs in the radial velocity and pressure structures in the convergent and divergent regions respectively, when the height of the constriction are varied.

**Corresponding author: E-mail: wiaokuyade@gmail.com;*

Keywords: Oscillatory flow; pulse amplitude; constriction height; convergent and divergent channels.

1 Introduction

Oscillatory flow of an incompressible viscous fluid through convergent and divergent channels has applications in engineering and biological systems.

The human cardiovascular system is infested by a number of diseases. An example of such is the atherosclerosis of the artery, which involves the hardening of the artery due to deposition of lipids (a generic name for esters) on its intimae/internal walls. The calcification of the lipids leads to lose of distensibility at the point of infection. Also, the progressive encroachment of the plague on the internal walls tends to block the passage of blood to other parts of the body. And, this imposes extra loads on the heart musculature [1,2]. To maintain the peripheral flow, the heart enlarges itself, and thus, increasing the amplitude of the pulse or pressure wave, which subsequently leads to abrupt rise in the flow variables [2,3]. More so, the encroachment of the plague leads to distortion of the tapered geometry of the artery to other forms, such as the idealized locally constricted channel (see [4,5]) and peristaltic channel (see [6,7]). This plague is found predominantly in the internal carotid artery which supplies blood to the brain; the coronary artery which supplies blood to the cardiac muscles, and the femoral artery which supplies blood to the lower limbs [1].

Rao and Devanathan [8] examined the fluid mechanical aspect of the pulsatile flow of an incompressible viscous fluid through tapered tube, locally constricted and peristaltic channels. They did not consider the flow behaviours in the regions before and after the peak of the stenos height, which are idealized as the convergent and divergent channels. Therefore, we are motivated to investigate the flow behaviours in these convergent-divergent channels using the same model.

There are several reports in literature on the flow of an incompressible viscous fluid through tubes of varying cross-sections. For example, [9] examined the characteristics of pulsating flow in a confined channel, and observed that a given rate of mass flow is obtained in oscillating motion under an average pressure gradient as in steady flow; [8] investigated the pulsating flow of an incompressible viscous fluid in tubes of varying cross-sections using the perturbation series expansion solutions which they developed, and observed that flow separation occurs in the wall shear stress structure in all geometries; [10] studied the steady laminar flow of an incompressible fluid in a channel of varying width with permeable boundaries, and observed that the fluid absorbed at the wall has a strong influence in reducing the occurrence of initial flow separation. Furthermore, [11] considered the pulsating flow an incompressible viscous fluid through stenotic vessels using the Reynolds-averaged Navier-Stokes approach, and predicted a wall shear stress peak at the throat of the stenosis with maximum values observed distal to the stenos where the flow separation occurred; [12] examined the effects of MHD field on a two-dimensional nonlinear flow of a incompressible viscous electrically conducting fluid through convergent-divergent channels using the Pade-Hermite approximations, and observed that critical values of various parameters and types of singularities exist for different choices of MHD effects. Similarly, [13] looked at the influence of heat and mass transfer on the flow of blood (which they considered as a Phan-Tien-Tanner fluid) through convergent tapering, divergent tapering and non-tapered arteries for different parameters of interest, and noticed among others, that the shearing stress at the throat of the stenos increases with an increase in the external parameter, volumetric flow and Weissenberg number; [14] presented an analysis of blood flow through carotid bifurcating arteries that are clogged with fats using the one way fluid-solid interaction, and showed the effects of the Newtonian and non-Newtonian behaviours on the flow.

The purpose of this paper is to address the effects of the amplitude of the pressure wave and height of constriction on the velocity, pressure and wall shear stress structures in the regions before and after the peak of the constriction using the perturbation series solutions of the form developed by [8].

This paper is organized in the following manner: section 2 is the methodology; section 3 gives the results and discussion, while section 4 holds the conclusions.

2 Methodology

We consider the flow of blood in axi-symmetric convergent and divergent channels whose radii vary slowly with the cross-sections. The fluid viscosity is a function of temperature. With the loss of distensibility, the channels now have rigid walls. At the entrance of the tube, we assume the flow to be fully developed and pulsating with a prescribed periodic frequency β and time average volume flux Q. If (R, θ, X) and (u, v, w) are the polar cylindrical orthogonal coordinates and vector components, respectively, assuming the flow is symmetrical about the X-axis, then for a two-dimensional flow situation the continuity, momentum and energy equations describing the flow are:

$$\frac{1}{\mathrm{R}}\frac{\partial}{\partial \mathrm{R}}(\mathrm{Ru})+\frac{\partial u}{\partial X} = 0 \tag{1}$$

$$\frac{\partial u}{\partial t}+u\frac{\partial u}{\partial R}+w\frac{\partial u}{\partial X}=-\frac{\partial p}{\partial R}+\upsilon\left(\frac{\partial^2 u}{\partial R^2}+\frac{1}{R}\frac{\partial u}{\partial R}+\frac{u}{R^2}+\frac{\partial^2 u}{\partial X^2}\right) \tag{2}$$

$$\frac{\partial w}{\partial \mathrm{t}}+\mathrm{u}\frac{\partial w}{\partial R}+w\frac{\partial w}{\partial X}=-\frac{1}{\rho}\frac{\partial \mathrm{p}}{\partial X}+\upsilon\left(\frac{\partial^2 w}{\partial \mathrm{R}^2}+\frac{1}{\mathrm{R}}\frac{\partial w}{\partial \mathrm{R}}+\frac{\partial^2 w}{\partial \mathrm{X}^2}\right) \tag{3}$$

where ρ the density, p the pressure, υ the kinematic viscosity of the fluid, and t is the time. R=0 is the centre or symmetric axis of the tube; $R=a_o(X,t)$, which is an arbitrary function of X and t is the cross-sectional radius of the tube; a_o is the characteristic radius of the tube, and t is the time.

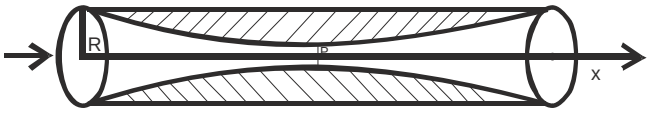

Fig. 1. The convergent and divergent models of the sclerotic artery

The boundary conditions are:

(i) $\mathrm{w} = 0,\ \frac{\partial u}{\partial \mathrm{R}}=0$ at R=0 (4)

(ii) there is no tangential motion at the wall of the tube ie:

$$u(a_o,t)=0 \text{ at } R=a_o(X,t) \tag{5}$$

(iii) the flux across a cross–section of the tube is prescribed as:

$$\int_0^{a_o(X,t)} dR \int_0^{2\pi} Rud\theta = 2\ \pi\psi_o\ (1+k\ e^{\ i\beta t}) \tag{6}$$

where ψ_o is a constant, k is the amplitude of the pulse which is assumed to be small, and β is the frequency of oscillation.

We eliminate the pressure terms in equations (2) and (3) by taking the $\frac{\partial}{\partial R}$ of equation (2) and $\frac{\partial}{\partial X}$ of equation (3), then subtracting the first result from the second one, we have

$$\frac{\partial}{\partial t}\left(\frac{\partial u}{\partial R}-\frac{\partial w}{\partial X}\right)+\frac{\partial u}{\partial X}\left(\frac{\partial u}{\partial R}-\frac{\partial w}{\partial X}\right)+\frac{\partial w}{\partial R}\left(\frac{\partial u}{\partial R}-\frac{\partial w}{\partial X}\right)=$$
$$\upsilon\left[\frac{\partial^2}{\partial X^2}\left(\frac{\partial u}{\partial R}-\frac{\partial w}{\partial X}\right)+\frac{\partial^2}{\partial R^2}\left(\frac{\partial u}{\partial R}-\frac{\partial w}{\partial X}\right)+\frac{1}{R}\frac{\partial}{\partial R}\left(\frac{\partial u}{\partial R}-\frac{\partial w}{\partial X}\right)-\frac{1}{R^2}\left(\frac{\partial u}{\partial R}-\frac{\partial w}{\partial X}\right)\right] \quad (7)$$

Also, the pressure expression in the axial direction can be obtained from equation (3), as

$$\frac{\partial p}{\partial X}=\upsilon\left(\frac{\partial^2 w}{\partial R^2}+\frac{1}{R}\frac{\partial w}{\partial R^2}+\frac{\partial^2 w}{\partial X^2}\right)-\left(\frac{\partial w}{\partial t}+u\frac{\partial w}{\partial R}+w\frac{\partial w}{\partial X}\right) \quad (8)$$

Introducing the stream function ψ and vortices Ω, respectively i.e.

$$\mathrm{u}=-\frac{1}{R}\frac{\partial \psi}{\partial R},\ \mathrm{w}=\frac{1}{\mathrm{R}}\frac{\partial \psi}{\partial X} \quad (9)$$

$$\Omega=\frac{\partial u}{\partial R}-\frac{\partial w}{\partial X}=\frac{1}{\mathrm{R}}\frac{\partial^2 \psi}{\partial R^2}-\frac{1}{R^2}\frac{\partial \psi}{\partial R}+\frac{1}{R}\ \frac{\partial^2 \psi}{\partial \mathrm{X}^2} \quad (10)$$

into equations (7) and (8), we have

$$\frac{\partial \Omega}{\partial t}-\frac{1}{R}\frac{\partial \Omega}{\partial X}\frac{\partial \psi}{\partial R}+\frac{1}{R}\frac{\partial \Omega}{\partial R}\frac{\partial \psi}{\partial X}+\frac{\Omega}{R^2}\frac{\partial \psi}{\partial X}=\upsilon\left[\frac{\partial^2 \Omega}{\partial X^2}+\frac{\partial^2 \Omega}{\partial R^2}+\frac{1}{R}\frac{\partial \Omega}{\partial R}-\frac{\Omega}{R^2}\right] \quad (11)$$

$$\frac{\partial p}{\partial X}=\upsilon\left(-\frac{1}{R}\frac{\partial^3 \psi}{\partial X^2 \partial R}-\frac{1}{R}\frac{\partial^3 \psi}{\partial R^3}-\frac{1}{R^2}\frac{\partial^2 \psi}{\partial R^2}\right)-\frac{1}{R^2}\frac{\partial \psi}{\partial R}\frac{\partial^2 \psi}{\partial X \partial R}+\frac{1}{R^2}\frac{\partial \psi}{\partial X}\frac{\partial^2 \psi}{\partial R^2}+\frac{1}{R}\frac{\partial^2 \psi}{\partial t \partial R} \quad (12)$$

with the boundary conditions as

$$\psi=0,\ \frac{1}{R}\frac{\partial \psi}{\partial X}=0,\ \frac{1}{R}\frac{\partial^2 \psi}{\partial R^2}-\frac{1}{R^2}\frac{\partial \psi}{\partial R}=0 \text{ at } \mathrm{R}=0 \quad (13)$$

$$\frac{\partial \psi}{\partial R}=0,\ \psi=\psi_o\left(1+ke^{i\beta t}\right) \text{at } R=a\left(X,t\right) \quad (14)$$

More so, we assume that the cross–section of the tube in the model vary in the axial direction, and for which we take a(X, t) = $a_o s$ (ε X/a_o , t), $r=R_0(1+\varepsilon f(x,t))$, 0 ≤ r ≤ 1, 0 ≤ x ≤ 1 where s is an arbitrary function of X; a is the variation in the r along the axial direction; $0<\varepsilon=\frac{a_o}{L}<<1$ is a small dimensionless parameter that characterizes the slow variation in the channel radius; L defines the channel

characteristic length; $\varepsilon = 0$ corresponds to a tube with constant radius. As ε increases from zero the variation of ψ in the axial direction depends upon ε X instead of X.

Similarly, introducing the following non-dimensionalized variables

$$r = \frac{R}{a_o}\ , x = \varepsilon \frac{X}{a_o},\ \ \mathrm{T} = \beta \mathrm{t},\ \ \phi\ (r, x, T) = \frac{\psi}{\psi_o},$$

$$\omega(r, x, T) = \frac{\Omega \mathrm{a}_o^3}{\psi_o}, \mathrm{Re} = \frac{\psi_o}{\mathrm{a}_o \upsilon},\ \eta\ = \frac{\beta}{a_o^2 \upsilon},\ \ \mathrm{a}_o = \frac{\mathrm{a}}{\mathrm{s}}$$

where Re is the Reynolds number of the flow, η is a dimensionless number for the frequency of oscillation, T is the dimensionless time, ε is the height of constriction, ϕ and ω are the dimensionless stream function and vortices respectively; into equations (8) - (12) respectively, we have

$$u = -\frac{1}{r}\frac{\partial \phi}{\partial \mathrm{r}} \tag{15}$$

$$w = -\frac{1}{r}\frac{\partial \phi}{\partial \mathrm{x}} \tag{16}$$

$$\omega = \frac{1}{r}\frac{\partial^2 \phi}{\partial r^2} - \frac{1}{r^2}\frac{\partial \phi}{\partial r} \tag{17}$$

$$\eta \frac{\partial \omega}{\partial T} + \frac{\mathrm{Re}}{r}\varepsilon\left(\frac{\partial \omega}{\partial r}\frac{\partial \phi}{\partial x} + \frac{\partial \omega}{\partial x}\frac{\partial \phi}{\partial r} + \frac{\omega}{r}\frac{\partial \phi}{\partial x}\right) = \frac{1}{r^2}\frac{\partial^2 \omega}{\partial r^2} + \frac{1}{r}\frac{\partial \omega}{\partial r} - \frac{1}{r}\omega \tag{18}$$

$$\frac{\partial p}{\partial X} = -\frac{\mathrm{Re}}{\varepsilon}\left(-\frac{1}{r}\frac{\partial^3 \phi}{\partial r^3} + \frac{1}{r^2}\frac{\partial^2 \phi}{\partial r^2}\right) + \frac{\eta}{\varepsilon r}\frac{\partial^2 \phi}{\partial r \partial T} \tag{19}$$

Equation (19) tends to suggest that the pressure field is of order $\frac{1}{\varepsilon}$. Also, the $O(\varepsilon)^2$ terms are assumed to be very small, therefore, they are neglected.

Similarly, the wall shear stress is given as

$\tau_w = \rho \upsilon \Omega$ (see [8]) yielding

$$\tau_w = \frac{1}{r}\frac{\partial^2 \phi}{\partial r^2} + \frac{1}{r^2}\frac{\partial \phi}{\partial r} \tag{20}$$

The boundary conditions become:

$$\phi = 0\ ,\ \frac{\partial \phi}{\partial x} = 0\ ,\ \frac{\partial}{\partial \mathrm{r}}\left(\frac{1}{\mathrm{r}}\frac{\partial \phi}{\partial \mathrm{r}}\right) = 0 \quad \text{at} \quad \mathrm{r} = 0 \tag{21}$$

$$\phi = 1\ +\ \mathrm{k}\ \mathrm{e}^{\ \mathrm{iT}},\ \frac{\partial \phi}{\partial \mathrm{r}} = 0 \quad \text{at} \quad \mathrm{r} = \mathrm{s}(\mathrm{x},\ \mathrm{T}) \tag{22}$$

Now, we shall seek for perturbation series solutions about the small parameter ε. In particular, we shall use the form developed by [8], and which is of the form:

$$f = f^{(o)} + ke^{iT}\,\overline{f}^{(o)} + \varepsilon\left(f^{(1)} + ke^{iT}\,\overline{f}^{(1)}\right) + \ldots \tag{23}$$

where f_n represents ω and ϕ.

Substituting equation (23) into equations (17), (18), (21) and (22), we have:

the zeroth order terms as

$$\omega^{(o)} = \frac{1}{r}\left(\frac{\partial^2\phi^{(o)}}{\partial r^2} - \frac{1}{r}\frac{\partial\phi^{(o)}}{\partial r}\right) \tag{24}$$

$$\omega^{(o)} = \frac{1}{r}\left(\frac{\partial^2\overline{\phi}^{(o)}}{\partial r^2} + \frac{1}{r}\frac{\partial\overline{\phi}^{(o)}}{\partial r}\right) \tag{25}$$

$$\frac{\partial^2\omega^{(o)}}{\partial r^2} + \frac{1}{r}\frac{\partial\omega^{(o)}}{\partial r} - \frac{1}{r^2}\;\omega^{(o)} = 0 \tag{26}$$

$$\frac{\partial^2\varpi^{(o)}}{\partial r^2} + \frac{1}{r}\frac{\partial\varpi^{(o)}}{\partial r} - \left(\lambda^2 + \frac{1}{r}\right)\varpi^{(o)} = 0 \tag{27}$$

where $\lambda^2 = i\eta$

with the boundary conditions are:

$$\left.\begin{aligned} &\phi^{(o)} = \overline{\phi}^{(o)} = 0 \\ &\frac{1}{r}\frac{\partial\phi^{(o)}}{\partial x} = \frac{1}{r}\frac{\partial\overline{\phi}^{(o)}}{\partial x} = 0 \\ &\frac{\partial}{\partial r}\left(\frac{1}{r}\frac{\partial\phi^{(o)}}{\partial r}\right) = \frac{\partial}{\partial r}\left(\frac{1}{r}\frac{\partial\overline{\phi}^{(o)}}{\partial r}\right) = 0 \end{aligned}\right\} \quad \text{at } r = 0 \tag{28}$$

$$\left.\begin{aligned} &\frac{\partial\phi^{(o)}}{\partial r} = \frac{\partial\overline{\phi}^{(o)}}{\partial r} = 0 \\ &\phi^{(o)} = \overline{\phi}^{(o)} = 1 \end{aligned}\right\} \quad \text{at} \quad r = s \tag{29}$$

while the first order terms are

$$\omega^{(1)} = \frac{1}{\mathrm{r}}\left(\frac{\partial^2\phi^{(1)}}{\partial \mathrm{r}^2} - \frac{1}{r}\frac{\partial\phi^{(1)}}{\partial r}\right) \tag{30}$$

$$\varpi^{(1)} = \frac{1}{\mathrm{r}}\left(\frac{\partial^2\bar{\phi}^{(1)}}{\partial \mathrm{r}^2} - \frac{1}{r}\frac{\partial\bar{\phi}^{(1)}}{\partial r}\right) \tag{31}$$

$$\frac{\partial^2\omega^{(1)}}{\partial \mathrm{r}^2} + \frac{1}{\mathrm{r}}\frac{\partial\omega^{(1)}}{\partial \mathrm{r}} - \frac{1}{\mathrm{r}}\ \omega^{(1)} = \frac{\mathrm{Re}}{r}\left[\frac{\partial\phi^{(o)}}{\partial r}\frac{\partial\omega^{(o)}}{\partial x} + \frac{\partial\phi^{(o)}}{\partial x}\left(\frac{\omega^{(o)}}{r} - \frac{\partial\omega^{(o)}}{\partial r}\right)\right] \tag{32}$$

$$\frac{\partial^2\varpi^{(1)}}{\partial r^2} + \frac{1}{r}\frac{\partial\varpi^{(1)}}{\partial r} - \left(\lambda^2 + \frac{1}{r^2}\right)\varpi^{(1)} = \frac{\mathrm{Re}}{r}\left[\frac{\partial\phi^{(o)}}{\partial r}\frac{\partial\omega^{(o)}}{\partial x} + \frac{\partial\bar{\phi}^{(o)}}{\partial r}\frac{\partial\omega^{(o)}}{\partial x}\right.$$
$$\left. - \frac{\partial\varpi^{(o)}}{\partial x}\left(\frac{\partial\varpi^{(o)}}{\partial r} - \frac{\varpi^{(o)}}{r}\right) - \frac{\partial\bar{\phi}^{(o)}}{\partial x}\left(\frac{\partial\omega^{(o)}}{\partial \mathrm{r}} - \frac{\omega^{(o)}}{r}\right)\right] \tag{33}$$

with boundary conditions

$$\left.\begin{aligned} &\phi^{(1)} = \bar{\phi}^{(1)} = 0 \\ &\frac{1}{r}\frac{\partial\phi^{(1)}}{\partial x} = \frac{1}{r}\frac{\partial\bar{\phi}^{(1)}}{\partial x} = 0 \\ &\frac{\partial}{\partial r}\left(\frac{1}{r}\frac{\partial\phi^{(1)}}{\partial r}\right) = \frac{\partial}{\partial r}\left(\frac{1}{r}\frac{\partial\bar{\phi}^{(1)}}{\partial r}\right) = 0 \end{aligned}\right\} \quad \text{at } \mathrm{r} = 0 \tag{34}$$

$$\left.\begin{aligned} &\frac{\partial\phi^{(1)}}{\partial r} = \frac{\partial\bar{\phi}^{(1)}}{\partial r} = 0 \\ &\phi^{(1)} = \bar{\phi}^{(1)} = 0 \end{aligned}\right\} \quad \text{at} \quad \mathrm{r} = \mathrm{s} \tag{35}$$

More so, by equation (22), equations (15), (16), (19) and (20) become

$$u = -\frac{1}{r}\frac{\partial\phi}{\partial \mathrm{r}} = -\frac{1}{r}\frac{\partial}{\partial \mathrm{r}}\left(\phi^{(o)} + ke^{iT}\phi^{(o)} + \varepsilon\phi^{(1)} + \varepsilon ke^{It}\phi^{(1)}\right) \tag{36}$$

$$w = \frac{1}{r}\frac{\partial\phi}{\partial \mathrm{x}} = \frac{1}{r}\frac{\partial s}{\partial \mathrm{x}}\cdot\frac{\partial\phi}{\partial \mathrm{s}} = \frac{1}{r}\frac{\partial s}{\partial \mathrm{x}}\cdot\frac{\partial}{\partial \mathrm{s}}\left(\phi^{(o)} + ke^{iT}\phi^{(o)} + \varepsilon\phi^{(1)} + \varepsilon ke^{It}\phi^{(1)}\right) \tag{37}$$

$$\frac{\partial p}{\partial x} = -\frac{\mathrm{Re}}{\varepsilon}\left[-\frac{1}{r}\frac{\partial^3 \phi^{(o)}}{\partial r^3} + \frac{1}{r^2}\frac{\partial^2 \phi^{(o)}}{\partial r^2} + ke^{iT}\left(-\frac{1}{r}\frac{\partial^3 \bar{\phi}^{(O)}}{\partial r^3} + \frac{1}{r^2}\frac{\partial^2 \bar{\phi}^{(O)}}{\partial r^2}\right)\right] \tag{38}$$

$$\tau_w = -\left(\frac{1}{r}\frac{\partial^2 \phi^{(O)}}{\partial r^2} + \frac{1}{r^2}\frac{\partial \phi^{(O)}}{\partial r}\right) - ke^{iT}\left(\frac{1}{r}\frac{\partial^2 \bar{\phi}^{(O)}}{\partial r^2} + \frac{1}{r^2}\frac{\partial \bar{\phi}^{(O)}}{\partial r}\right) - \varepsilon\left(\frac{1}{r}\frac{\partial^2 \phi^{(1)}}{\partial r^2} + \frac{1}{r^2}\frac{\partial \phi^{(1)}}{\partial r}\right) - \varepsilon k e^{iT}\left(\frac{1}{r}\frac{\partial^2 \bar{\phi}^{(1)}}{\partial r^2} + \frac{1}{r^2}\frac{\partial \bar{\phi}^{(1)}}{\partial r}\right) \tag{39}$$

The analyses of the solutions show that the non-steady part is very insignificant.

By exhaustive algebraic operations, the solutions of the zeroth order equations (23) - (26), (29) - (32) and (35) - (38), are:

$$\phi^{(o)} = 2\left(\frac{r}{s}\right)^2 - \left(\frac{r}{s}\right)^4 \tag{40}$$

$$\bar{\phi}^{(o)} = \frac{r^2}{\lambda s^2 I_2(\lambda s)}\left[I_o(\lambda s) - I_o(\lambda r) + I_2(\lambda r)\right] \tag{41}$$

$$\omega^o = -\frac{8}{s^3}\left(\frac{r}{s}\right) \tag{42}$$

$$\bar{\omega}^{(O)} = -2\frac{\lambda I_1(\lambda r)}{s^2 I_2(\lambda s)} \tag{43}$$

$$\phi^{(1)} = -\frac{\mathrm{Re}}{s}\frac{\partial s\varepsilon}{\partial x}\left[\frac{1}{9}\left(\frac{r}{s}\right)^8 - \frac{2}{3}\left(\frac{r}{s}\right)^6 + \left(\frac{r}{s}\right)^4 - \frac{4}{9}\left(\frac{r}{s}\right)^2\right] \tag{44}$$

$$\bar{\phi}^{(1)} = \frac{4\,\mathrm{Re}}{\lambda^4 s^4}\frac{\partial s}{\partial x}\left\{\frac{I_1(\lambda r)}{s\lambda^2 I_2(\lambda s)}\left[\left(\frac{2}{3}s^4\lambda^4 - 5s^2\lambda^2 - 32\right)\lambda I_1^2(\lambda s) + \left(\frac{1}{2}s^2\lambda^2 + 16\right)\lambda^2 s I_o(\lambda s) I_1(\lambda s) + \left(\frac{2}{3}\lambda^4 s^4 + 12\lambda^2 s^2 - 128\right)\frac{I_1(\lambda s)}{s} + \left(64 - 6\lambda^2 s^2 - \frac{1}{4}\lambda^4 s^4\right)\lambda I_o(\lambda s)\right]\right\} \tag{45}$$

$$\omega^{(1)} = \frac{8\,\mathrm{Re}}{s^4}\frac{\partial s}{\partial x}\left[\frac{2}{3}\left(\frac{r}{s}\right)^5 - 2\left(\frac{r}{s}\right)^3 + \left(\frac{r}{s}\right)\right] \tag{46}$$

$$\bar{\omega}^{(1)} = 4\frac{\mathrm{Re}}{\lambda^4 s^4}\frac{\partial s}{\partial x}\left\{\frac{1}{\lambda^2 I^2(\lambda s)}\left[\left(\frac{2s^4\lambda^4}{3}-5s^2\lambda^2-32\right)\lambda I_1^2(\lambda s)\right]\right.$$
$$\left.+\left[I_o(\lambda r)\left(\lambda s^2 r-\frac{\lambda r^2}{3}\right)I_1(\lambda s)-\frac{r^3}{s}+2sr\right]\right\} \quad (47)$$

$$u = -\frac{4}{s^2}+\frac{4r^2}{s^4}-\frac{ke^{iT}}{\lambda s^2 I_2(\lambda s)}2\left(I_o(\lambda s)-I_o(\lambda r)+\lambda r I_1(\lambda r)\right)$$
$$+\frac{\varepsilon\,\mathrm{Re}}{s^3}\frac{\partial s}{\partial x}\left[\frac{8}{9}\left(\frac{r}{s}\right)^6-4\left(\frac{r}{s}\right)^4+4\left(\frac{r}{s}\right)^2-18\right]$$
$$+\frac{\varepsilon k e^{iT}}{r\lambda^4 s^6 I_2(\lambda s)}4\,\mathrm{Re}\frac{\partial s}{\partial x}\left\{\frac{I_o(\lambda r)}{s\lambda I_2(\lambda s)}\left[\begin{array}{l}\left(\frac{2}{3}s^4\lambda^4-s5^2\lambda^2-32\right)\lambda I_1^2(\lambda s)\\+\left(\frac{1}{2}s^2\lambda^2+16\right)\lambda^2 s I_o(\lambda s)\\+\left(\frac{3}{2}s^4\lambda^4-12s^2\lambda^2-128\right)\frac{I_1(\lambda s)}{s}\\+\left(64-6s^2\lambda^2-\frac{1}{4}s^4\lambda^4\right)I_o(\lambda s)\end{array}\right]\right.$$
$$\left.+\lambda^4 r^2\left(\frac{3}{2}s^2-\frac{8}{\lambda^2}\right)I_1(\lambda r)I_1(\lambda s)-\frac{4}{3}\lambda^3 r^2 I_o(\lambda r)I_1(\lambda s)+..\right\} \quad (48)$$

$$w = \left(4\frac{r^3}{s^5}-2\frac{r}{s^3}\right)\frac{\partial s}{\partial x}-\frac{ke^{iT}r}{sI_2^2(\lambda s)}\frac{\partial s}{\partial x}\left[I_o(\lambda s)I_1(\lambda s)-I_1(\lambda s)I_o(\lambda r)+I_1(\lambda s)I_2(\lambda r)\right]$$
$$+\varepsilon\frac{\mathrm{Re}}{s^3}\left(\frac{\partial s}{\partial x}\right)^2\left[\left(\frac{r}{s}\right)^7-\frac{14}{3}\left(\frac{r}{s}\right)^5+5\left(\frac{r}{s}\right)^3-27\left(\frac{r}{s}\right)\right]$$
$$+\varepsilon k e^{iT}\left\{\begin{array}{l}\frac{4\,\mathrm{Re}}{r\lambda^6}I_2(\lambda r)\frac{\partial s}{\partial x}\left[\begin{array}{l}\frac{2}{3}\lambda^6\left(2s^3 I_o(\lambda s)I_1(\lambda s)I_2^2(\lambda s)+\frac{s^2}{\lambda}\left(I_1^2(\lambda s)I_2^2(\lambda s)\right)\right)\\-5\lambda^4\left(2s^5 I_o(\lambda s)I_1(\lambda s)I_2^2(\lambda s)-\frac{s^4}{\lambda}I_1^2(\lambda s)I_2^2(\lambda s)\right)\\-32\lambda^2\left(2s^7 I_o(\lambda s)I_1(\lambda s)I_2^2(\lambda s)-3\frac{s^6}{\lambda}I_1^2(\lambda s)I_2^2(\lambda s)\right)\end{array}\right]\\+\frac{4\,\mathrm{Re}\,r}{s4I_2^2(\lambda s)}I_2(\lambda r)\frac{\partial s}{\partial x}\left[\begin{array}{l}I_o(\lambda s)-\frac{4}{3s^2}\left(I_o(\lambda s)-\frac{2I_1(\lambda s)}{\lambda s}\right)\\-\frac{8}{\lambda^2 s^2}\left(I_o(\lambda s)-\frac{2I_1(\lambda s)}{\lambda s}\right)\end{array}\right]\end{array}\right. \quad (49)$$

$$p=\frac{1}{\varepsilon}\left[\frac{36x}{s^4}-\frac{ke^{iT}x}{s^2I_2(\lambda r)}\left[\frac{10}{r}I_1(\lambda r)+7\lambda rI_o(\lambda r)-\left(\lambda^2r+\lambda^2r^2\right)I_1(\lambda r)\right]\right]\quad 0\le x\le 1 \tag{50}$$

$$\tau_w=\frac{8}{s^2}-\frac{ke^{iT}x}{s^2I_2(\lambda s)}\left(\lambda s^2I_o(\lambda s)+4sI_1(\lambda s)\right)+\varepsilon\frac{8}{3s^3}\mathrm{Re}\frac{\partial s}{\partial x}+$$

$$\frac{\varepsilon ke^{iT}}{\lambda^4s^6I_2(\lambda r)}\mathrm{Re}\frac{\partial s}{\partial x}\left\{\frac{I_1(\lambda s)}{s^2I_2(\lambda s)}\left[\begin{array}{l}\left(\frac{2}{3}s^4\lambda^4-s^2\lambda^2-32\right)I_1^2(\lambda s)\\+\left(\frac{1}{2}s^2\lambda^2+16\right)\lambda^2sI_o(\lambda s)I_1(\lambda s)\\\left(\frac{3}{2}s^4\lambda^4-12s^2\lambda^2-128\right)\frac{I_1(\lambda s)}{s}\\+\left(64-6s^2\lambda^2-\frac{1}{4}s^4\lambda^4\right)I_o(\lambda s)\end{array}\right]\right.$$
$$\left.+\lambda^4\left(\frac{4s}{3}-6s^3+\frac{32s}{\lambda^2}\right)I_1^2(\lambda s)\right\} \tag{51}$$

where $I_o(\lambda r)$, $I_1(\lambda r)$, $I_2(\lambda r)$, $I_o(\lambda s)$, $I_1(\lambda s)$ and $I_2(\lambda s)$ are the modified Bessel function of order zero, one, two, respectively. It is worthy to note that the solutions to equations (31) and (33) as expressed in equations (45) and (47) are culled and developed from [8], p. 206.

Furthermore, the geometries under consideration are: the convergent channel $s=e^{-x/2}$, and divergent channel $s=e^{x/2}$.

3 Results and Discussion

We considered the flow of blood through a stenos artery with emphasis on the effects of pressure wave amplitude and height of constriction on the overall flow structure in the regions before and after the peak of the constriction. These two regions under consideration approximate the convergent and divergent channels, as shown in Fig. 1. The analyses of the results show that variations in the amplitude and height of the constriction have tremendous effects on the flow structure. To this end, using Maple 12 computational software and the following physically realistic parameters: $T=\pi/4$; $\lambda=2$; k = 0.01, 0.03, 0.05, 0.07; ε = 0.01, 0.03, 0.05, 0.07; Re= 10, 100, 500, 1000 we obtained the results shown in Figs. 2 – 17. These figures show the profiles of the computational results for the velocities pressure and wall shear stress. The profiles show that increase in the amplitude decreases the axial velocity and axial pressure (see Figs. 2, 3, 6 and 7), but increases the radial velocity and wall shear stress (see Figs. 4, 5, 8 and 9). Blood flow in a normal artery is laminar and Poiseuille. But due to the stenosis, the arterial channel is blocked moderately or severely. For this, the heart enlarges itself to maintain the peripheral flow. The enlargement of the heart leads to increase in the amplitude of the pulse or pressure wave. And, the increase in the amplitude energizes the flow variables in the direction of the increase, which in this case, the radial velocity and wall shear stress. This accounts for what is seen in Figs. 4, 5, 8 and 9. On the other hand, the increase in the amplitude reduces the axial velocity and axial pressure as seen in Figs. 2, 3, 6 and 7. This could be due to the increase in the radial velocity.

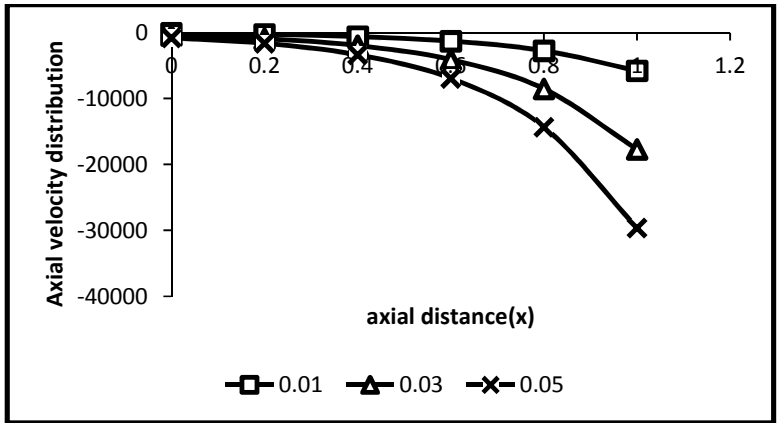

Fig. 2. Axial velocity-amplitude (k) profiles in a convergent channel

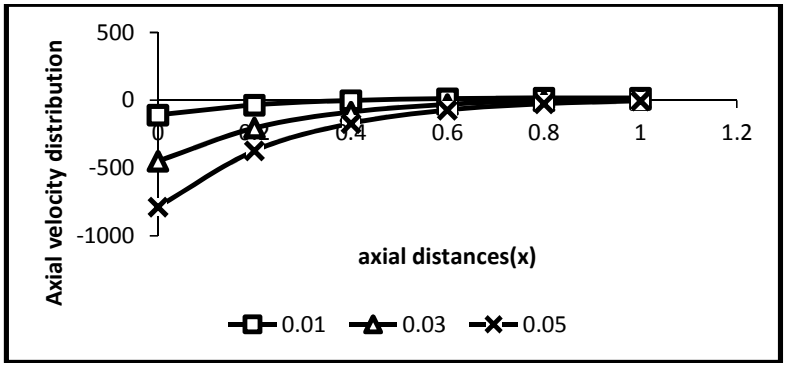

Fig. 3. Axial velocity-amplitude (k) profiles in a divergent channel

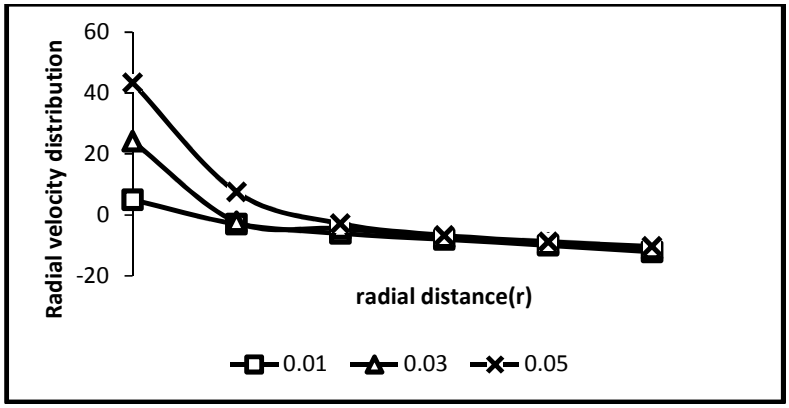

Fig. 4. Radial velocity-amplitude (k) profiles in a convergent channel

Furthermore, the profiles show that the height of the constriction decreases the axial velocity (see Figs. 10 and 11), while it increases the axial pressure and wall shear stress (see Figs. 14, 16 and 17). As said above, blood flow in the artery is laminar, Poiseuille and fully developed. It moves with the velocity with which it is released from the heart. As it gets to the region of constriction, the flow pattern changes. The blockage caused by the stenos reduces the axial pressure as shown in Fig. 10 and Fig. 11.

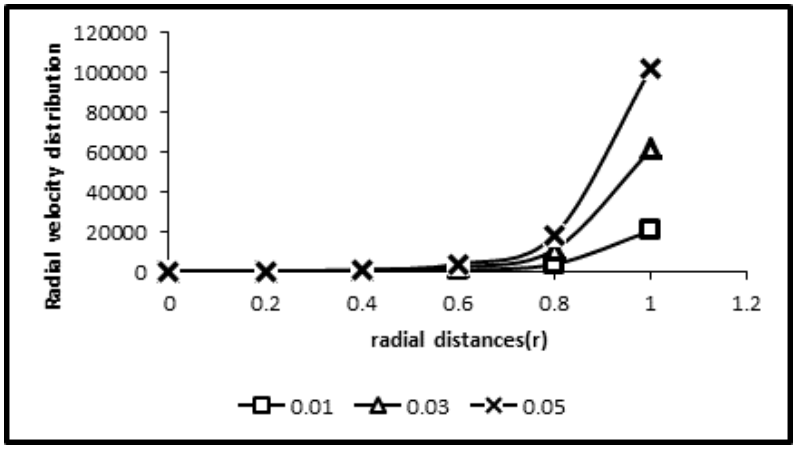

Fig. 5. Radial velocity-amplitude (k) profiles in a divergent channel

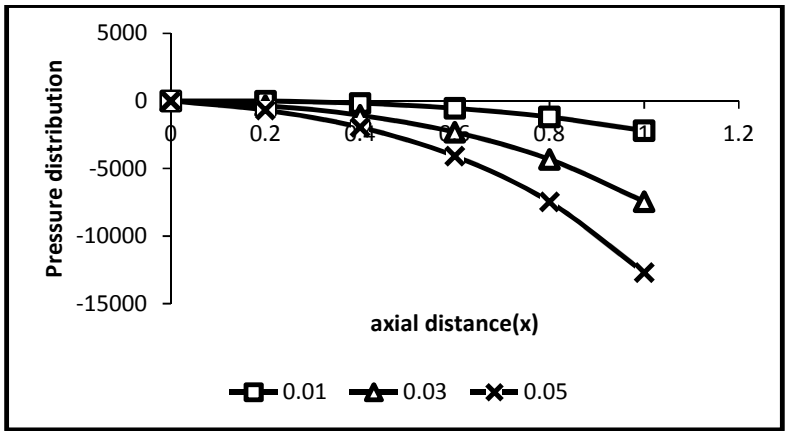

Fig. 6. Pressure-amplitude (k) profiles in a convergent channel

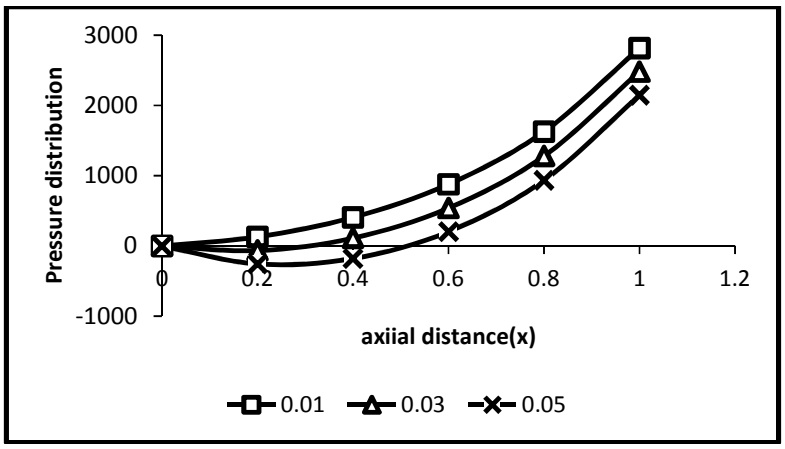

Fig. 7. Pressure-amplitude (k) profiles in a divergent channel

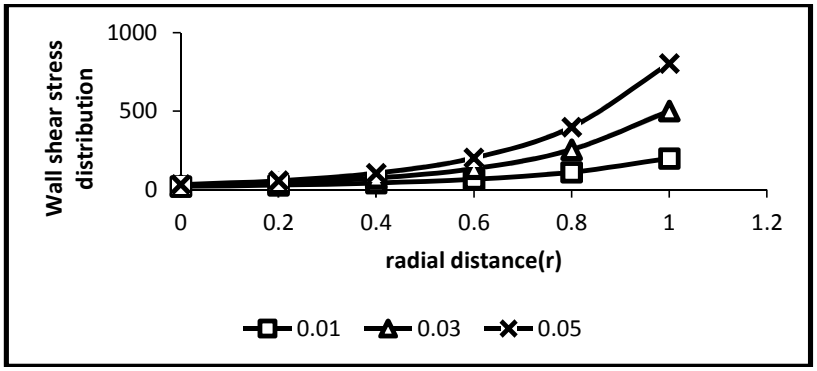

Fig. 8. Wall shear stress-amplitude (k) profiles in a convergent channel

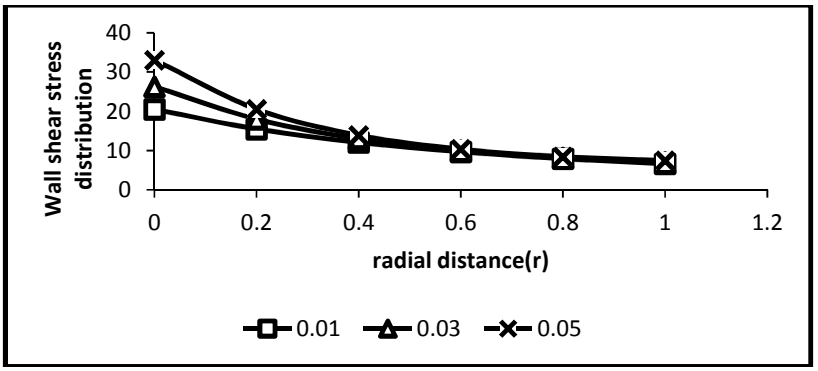

Fig. 9. Wall shear stress-amplitude (k) profiles in a divergent channel

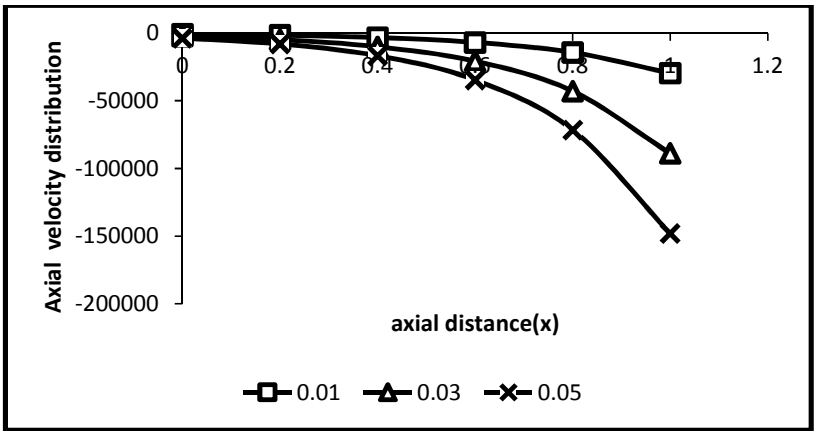

Fig. 10. Axial velocity-height of constriction (ε) profiles in a convergent channel

More so, the changes in the geometrical configuration affect the flow. In particular, for the convergent channel, as the geometry thins down exponentially, the pressure factor increases, and subsequently, the velocities and wall shear stress increase. It is also seen that in the divergent channel whose geometry increases exponentially, the radial velocity, axial pressure and wall shear stress are increased. The increase

could be due to the influence of the flow situations in the convergent channel. All these account for the results in Figs. 13, 14, 16 and 17.

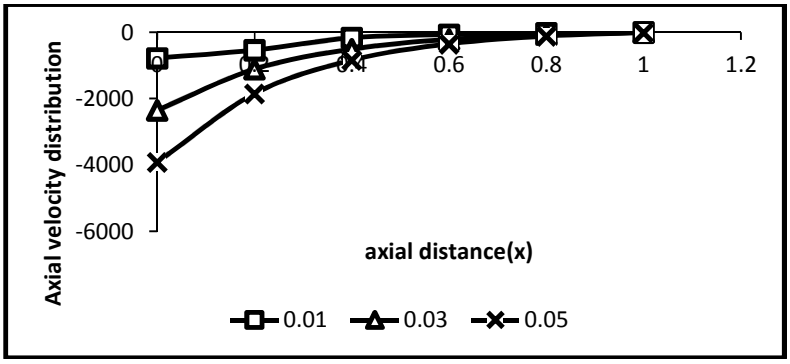

Fig. 11. Axial velocity-height of constriction (ε) profiles in a divergent channel

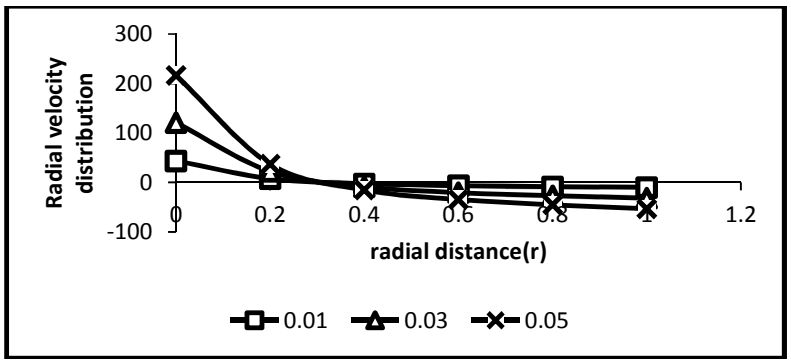

Fig. 12. Radial velocity-height of constriction (ε) profiles in a convergent channel

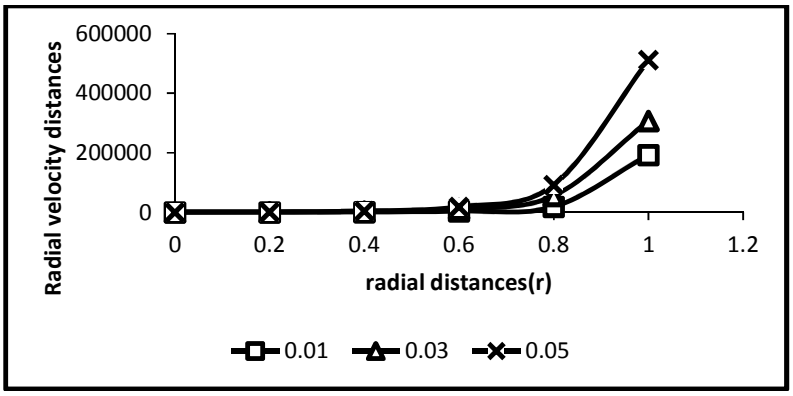

Fig. 13. Radial velocity-height of constriction (ε) profile in a divergent channel

Similarly, a special feature called the flow separation occurs in the radial and pressure structures at $r \leq 0.3$ and $r \leq 0.46$ for $T=\pi/4$, respectively (see Figs. 12 and 15). Initially, the radial velocity and pressure increase with the height of constriction drop at these points, and then the flow pattern changes such that these variables decrease as the height of constriction increases. The occurrence of the flow separation (which is in

agreement with [8]) is due to the adverse flow conditions at such points. [8] adduced that it is due to viscous effects.

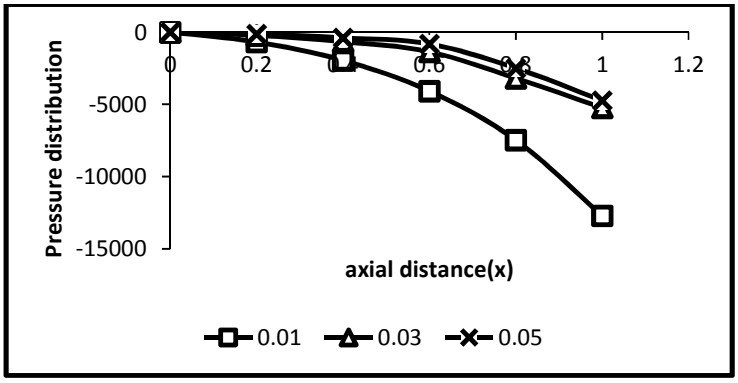

Fig. 14. Pressure-height of constriction (ε) profiles in a convergent channel

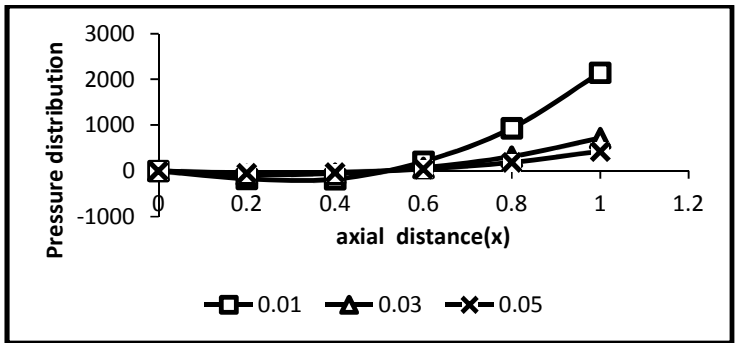

Fig. 15. Pressure-height of constriction (ε) profiles in a divergent channel

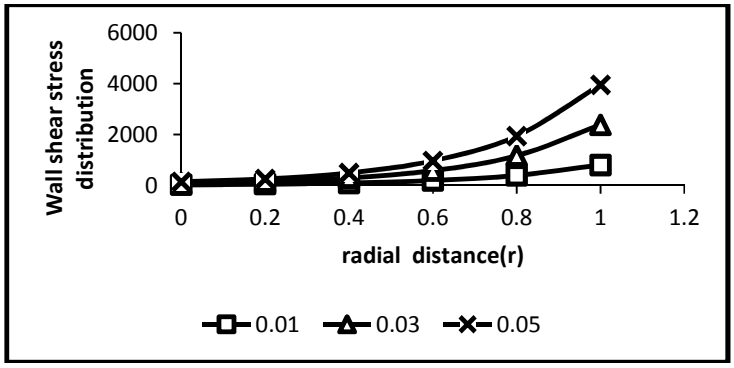

Fig. 16. Wall shear stress-height of constriction (ε) profiles in a convergent channel

The overall analyses show that the axial velocity drops as the pulse amplitude and height of constriction increase. This has some health implications on the stenotic patient. The drop in the axial velocity leads subsequently to a drop in the rate at which the rejuvenated blood which bears oxygen and food nutrients is transported to other parts of the body, thus causing cells starvation.

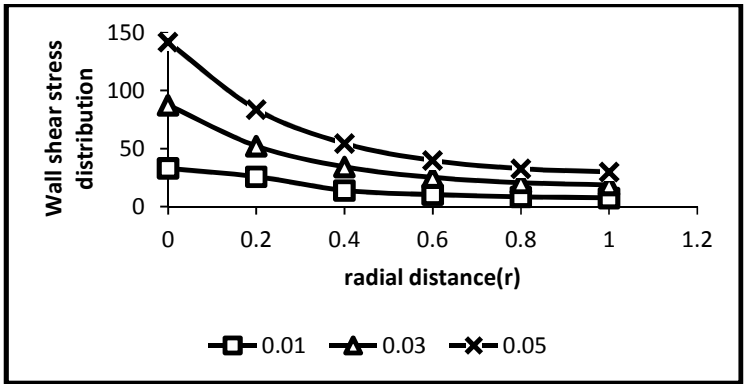

Fig. 17. Wall shear stress-height of constriction (ε) profiles in a divergent channel

4 Conclusions

The analyses of the results indicate that the pulse amplitude and height of constriction reduce the axial velocity and pressure but increase the radial velocity and wall shear stress. The occurrence of flow separation in the radial velocity and pressure structures are due to some adverse flow situations at such points. Furthermore, the drop in the axial velocity has some physiological implications on the stenotic patient.

Acknowledgement

We are thankful to the Springer Publishers. By the permission of the Springer Science + Business Media, the solutions to equations (31) and (33) as seen in equations (45) and (47) are adopted from [8].

Competing Interests

Authors have declared that no competing interests exist.

References

[1] Mittal R, Simmons SP, Najjar F. Numerical study of pulsatile flow in a constricted channel. Journal of Fluid Mechanics. 2003;485:337-378.

[2] Anliker M, Rockwell RL, Odgen, E. Non-linear analysis of flow pulses and shock waves in arteries, 1 and 2. Z. Angnew. Maths Physics. 1971;22:217-246, 563-581.

[3] Ayeni RO, Akinrelere AE. On temperature factor and effect of viscosity on blood temperature in arteries. Journal of Theoretical Biology. 1984;109:479-487.

[4] Burns JC, Parkes T. Flow of incompressible fluid in peristaltic tubes. Journal of Fluid Mechanics. 1967;29:731.

[5] Shapiro AH, Jaffins MY, Weinburg SL. Flow of incompressible fluid in peristaltic tubes. Journal of Fluid Mechanics. 1969;37:409.

[6] Lee JS, Fung YC. Flow of incompressible fluid in locally constricted tubes. Journal of Applied Mechanics. 1970;37:9.

[7] Yin FC, Fung YC. Flow of incompressible fluid in peristaltic tubes. Journal of Applied Mechanics. 1971;47:93.

[8] Rao AR, Devanathan R. Pulsatile flow in tubes of varying cross-sections. Z. Angew Maths Physics. 1973;24:203-213.

[9] Uchida S. Pulsating viscous flow superimposed on the steady-laminar motion of incompressible fluid in a circular pipe. Z. Angew. Maths Physics. 1956;2:403-421.

[10] Makinde OD. Laminar flow in a channel of varying width with permeable boundaries. Romanian Journal of Physics. 1995;4:157-165.

[11] Varghese S, Franel S. Numerical analysis of flow through a severely stenotic vessel. Journal of Biomechanical Engineering. 2003;125:445-465.

[12] Alam MS, Khan MAH. Critical behaviour of the MHD flow in convergent-divergent channels. Journal of Naval Architecture and Marine Engineering. 2010;7:83-89.

[13] Noreen SA, Nadeen S, Changhoon L. Influence of heat and mass transfer on a Phan-Tien-tanner fluid model for blood flow through a tapered artery with a stenosis. 2012;7(43):3737-3750.

[14] Pratumwal Y, Limtrakarn W, Premvaranon P. The analysis of blood flow past carotid bifurcation by using the one-way fluid-solid interaction technique (fsi). Transactions of the TSME. Journal of Research and Applications in Mechanical Engineering. 2014;57-64.

Peer-review history:
The peer review history for this paper can be accessed here (Please copy paste the total link in your browser address bar)
http://sciencedomain.org/review-history/13474